CELLULOSE NANOCRYSTALS BASED ON PINEAPPLE LEAF FIBERS IN HEMOPERFUSION APPLICATIONS FOR CREATININE REMOVAL: BATCH METHOD ADSORPTION STUDY

Yanuardi Raharjo[1*], Handoko Darmokoesoemo[2], Amelia Julia Tria Fetty[2], Rizky Abdul Aziz[2], Fara Salsabila[2], Ervina Fadhilatul Ishma[2]
[1]Composite Materials Technology and the Applications Research Group, Chemistry Department, Faculty of Science and Technology, Universitas Airlangga, Surabaya 60115, Indonesia
[2]Department of Chemistry, Faculty of Science and Technology, Universitas Airlangga, Surabaya 60115, Indonesia
[*]Email: yanuardiraharjo@fst.unair.ac.id

Received 05 September 2024
Accepted 19 November 2024

Abstract

Kidney failure is a major global cause of mortality, often resulting from the buildup of uremic toxins like creatinine. Creatinine serves as an indicator for assessing treatment needs in kidney failure patients. Hemoperfusion, a treatment based on the adsorption of toxins, has shown promise when using cellulose nanocrystals (CNCs) as adsorbents. CNCs derived from pineapple leaf fibers offer unique advantages due to their abundance of active sites, high adsorption capacity, and strong binding affinity. This study investigates the efficiency of CNCs in reducing creatinine levels, with the reduction attributed to the binding of creatinine to CNC hydroxyl groups. Characterization of CNCs was performed using PSA, XRD, FTIR, and SEM-EDX techniques, while the residual creatinine was quantified via UV-Vis spectrophotometry, utilizing a picric acid complex under alkaline conditions and measured at 485 nm. Optimal conditions were found with a stirring speed of 210 rpm, 120-minute contact time, and 10 mg/L creatinine concentration, resulting in an adsorption capacity (Q_{ads}) of 2.572 mg/g. The CNC adsorbent demonstrated hemocompatibility, with an APTT blood coagulation time of 31.3 seconds. These findings suggest that CNCs could be highly effective in developing safer, efficient hemoperfusion systems for managing kidney failure.

Keywords*: cellulose nanocrystals, creatinine, hemoperfusion, pineapple leaf fiber.*

Introduction

In the 21st century, chronic kidney failure has become one of the leading causes of death (Kovesdy, 2022). Chronic kidney failure is a condition in which patients experience a sudden negative change in blood quality due to the accumulation of uremic toxins in the body. Creatinine is one of the uremic toxins that can be used as an indicator to determine whether a person with kidney failure requires medical treatment (Alfonso *et al.*, 2016).

The treatment for chronic kidney failure patients commonly used in the medical field includes renal replacement therapy and kidney transplantation. However, only a small portion of chronic kidney failure patients have the opportunity to undergo kidney transplantation due to the scarcity of kidney donors, biological incompatibility, and high costs (Levey and Coresh, 2012). Therefore, renal replacement therapy becomes the only option for the majority of chronic kidney failure patients. Renal replacement therapy can be classified into two methods: hemodialysis and hemoperfusion. Hemodialysis is an effective and commonly used treatment

for chronic kidney failure (Cui *et al.*, 2016). According to Nguyen *et al.* (2021), hemodialysis can only remove about 75% and 66% of accumulated urea and creatinine in the body.

The adsorption method has been commonly used to remove urea, creatinine, and other toxins from simulated solutions. Biologically based adsorbents have attracted attention due to their biocompatibility, degradability, smooth and porous surface with a large specific surface area. Most commercial hemoperfusion adsorbents are made from activated carbon (AC) and resin. However, these conventional adsorbents have low removal efficiency and are unable to meet the growing demands for CKD patient treatment (Wang *et al.*, 2023). In addition to AC and resin, sol-gel can be used as an adsorbent for creatinine in hemoperfusion. Previous research on imprinted poly(tetraethoxysilanol) sol-gel adsorbent was used to adsorb creatinine but only produced an adsorption capacity of 0.82 mg/g (Tsai *et al.*, 2011). Therefore, it is essential to develop new hemoperfusion adsorbents with high efficiency and a broad-spectrum adsorption capability for various uremic toxins (Wang *et al.*, 2023). Another biologically-based adsorbent material that can be used for uremic toxin adsorption is cellulose. Cellulose has abundant active adsorption sites, a simple preparation process, high adsorption capacity, high crystallinity, high efficiency, stable recyclability, and easy separation (Jiang *et al.*, 2023).

Nanocellulose has abundant active adsorption sites, higher adsorption capacity, and binding affinity compared to macro-structured cellulose due to its larger specific surface area, higher strength modulus, and greater mechanical strength. Two main types of nanocellulose can be obtained: cellulose nanocrystals (CNCs), which are small, rigid cellulose rods produced through acid treatment, and cellulose nanofibrils, which are tube-shaped cellulose aggregates with irregular parts primarily produced through milling processes (Faria *et al.*, 2020). According to Sun *et al.* (2014), cellulose nanocrystals exhibit unique features, such as high strength and modulus (10 and 150 GPa, respectively), low density (1.6 g/cm^3), and high specific surface area (150 m^2/g). CNCs are a recent class of renewable, bio-derived nanomaterials which recognized as super-adsorbents due to their abundance of surface hydroxyl groups, versatile functionalities, and adaptable surface chemistry. Today, CNC's unique properties have enabled extensive applications in fields such as biomedicine, drug delivery, 3D printing, food packaging, materials engineering, polymer reinforcement, electronics, water purification, and pollutant removal (Lim and Foo, 2024). Polysaccharides derived from natural sources, such as CNCs, appear to be promising candidates for hemoperfusion adsorbents, as they inherit excellent hemocompatibility from their natural polysaccharide origin. CNCs also have a high surface-to-volume ratio due to their nanoscale dimensions, which can be further enhanced by modifying their surface chemistry. This large surface area allows CNCs to act as efficient adsorbents, capable of capturing various toxic molecules, heavy metals, and uremic toxins from the blood. Depending on preparation and source, the specific surface area can range between 100-200 m^2/g, making CNCs suitable for hemoperfusion systems (Faria *et al.*, 2020). However, using of CNCs as adsorbents in hemoperfusion is still relatively limited (Li *et al.*, 2022).

Pineapple is widely available and inexpensive in Indonesia. According to data from the Central Statistics Agency, pineapple production in Indonesia reached 3.2 million tons in 2022. The higher the pineapple production, the greater the waste produced (Saragih *et al.*, 2023). Due to its high availability and low cost, pineapple residue from consumption

becomes a viable alternative for nanocellulose production processes. A significant amount of residue is generated from pineapple consumption, including discarded peels and leaves, yet only limited research has utilized these for nanoparticle production. This natural fiber holds high potential for this purpose due to its cellulose content (70-82%) and excellent mechanical properties, making it more attractive to researchers than other lignocellulosic sources (Faria *et al.*, 2020). Based on the research of Faria *et al.*(2020), the results of the synthesis of CNCs from pineapple crown fiber in this study showed that the process used was very effective. This study found that the pretreatment steps, such as mercerization with heating and the use of 40% sulfuric acid at the hydrolysis stage, gave the best results. This process successfully produced complete hydrolysis of the fiber mass with fully bleached particles, indicating good potential for utilizing this agricultural waste. The process of extracting cellulose from pineapple leaf fibers can increase the crystalline fraction of cellulose, which enhances thermal stability and mechanical properties, making it more suitable for high-performance applications (Gadzama *et al.*, 2020).

This study, synthesizes cellulose nanocrystals from pineapple leaf fibers as raw material. Using the batch method, the synthesized cellulose nanocrystals were used to adsorb the creatinine solution, with optimizing stirring speed, contact time, and feed solution concentration.

Research Methods

Materials

The materials used in this study were pineapple leaf fibers, NaOH (Sigma-Aldrich, America), H_2O_2 (Sigma-Aldrich, America), H_2SO_4 (Sigma-Aldrich, America), glacial acetic acid (Merck, Germany), creatinine (Sigma-Aldrich, America), and picric acid (Sigma-Aldrich, America).

Instrumentation

This research utilized various tools, including an orbital sieve shaker Oregon KJ 201 BD Kangjian, a hotplate magnetic stirrer Thermo Scientific USA, and a UV 1800 (UV-Vis Spectrophotometer Shimadzu).

Procedure

1) Preparation and pretreatment of pineapple leaf fibers

   The preparation and pretreatment was adapted from Faria *et al.* (2020) and applied to previously washed, dried, and cut pineapple fibers. Then, mercerization was performed by adding 5% NaOH solution (w/v) into a beaker containing 5 grams of pineapple leaf fiber, stirred with a magnetic stirrer at 70°C for 1 hour. After that, the pineapple leaf fiber was washed until neutral and dried. The pineapple leaf fiber was then bleached by adding 100 mL of a 24% H_2O_2 solution (v/v) and a 4% NaOH solution (w/v) in a 1:1 ratio to a beaker containing 5 grams of fiber, stirred vigorously with a magnetic stirrer at 50 °C for 2 hours. The fiber was subsequently washed until neutral and dried. The next step was delignification by adding fiber to a 3% NaOH solution in a 1:10 (w/v) ratio, then stirred and heated at 50 °C for 2 hours using a magnetic stirrer. Finally, the pineapple leaf fiber was washed until it was neutral and dried.

2) Acid hydrolysis

   The acid hydrolysis process was determined based on the work of Faria *et al.* (2020). 5 grams of delignified pineapple leaf fiber were added to 100 mL of 30% H_2SO_4 solution in a beaker and stirred at 50 °C for 2 hours. After 2 hours, the acid hydrolysis reaction was stopped by adding distilled water to the sample solution at a 1:5 (v/v) ratio. The sample was then homogenized using a magnetic stirrer for 2 minutes. Next, the sample was

neutralized and dried in an oven at 60 °C for 24 hours.

3) Chemical characterization

The content of moisture, ash, lignin, and alpha-cellulose in fibers before and after pretreatment were determined based on the work of Faria *et al.* (2020). Characterization of the obtained cellulose nanocrystals was conducted using a Particle Size Analyzer (PSA), X-ray diffraction (XRD), Fourier Transform Infrared Spectroscopy (FTIR), and Scanning Electron Microscopy with Energy Dispersive X-Ray Spectroscopy (SEM-EDX).

a. Moisture content

2 gram of pineapple leaf fiber were heated in an oven at 105 °C for 3 hours, then cooled to room temperature and weighed. The weighed pineapple leaf fiber was placed back in the oven at the same temperature for 30 minutes, repeating the process until a constant sample weight was achieved. The moisture content was calculated using Equation (1), where MCU is the mass of (empty beaker - (beaker + wet sample)), MCS is the mass of (empty beaker - (beaker + dry sample)), MU is the mass of the wet sample, and TU% is the moisture content of the sample.

$$TU\% = [(MCU - MCS)/MU] \times 100 \quad (1)$$

b. Ash content

2 gram of pineapple leaf fiber of pineapple leaf fiber were placed in a porcelain crucible previously calcined at 600°C for 30 minutes and cooled in a desiccator. The sample was then gradually heated in a muffle furnace to reach a temperature of 600°C for 3 hours and cooled to 200°C. The cooled sample was weighed. The ash content was calculated using Equation (2), where MCF is the mass of the calcined porcelain crucible with the sample, MC is crucible mass, MF is the mass of the sample, and TC% is the ash content.

$$TC\% = \left[\frac{(MCF - MC)}{MF}\right] \times 100 \quad (2)$$

c. Lignin content

15 mL of 72% sulfuric acid at 10-15°C was slowly added to 1 gram of fiber and allowed to sit for 2 hours. The sample was placed into an Erlenmeyer flask containing 575 mL of water. The Erlenmeyer flask was connected to a condenser and heated using a heating blanket for 4 hours. The solution was allowed to stand for 24 hours for the undissolved lignin to decant, then filtered and washed with hot water to remove acid residues. The filtered sample was then heated in an oven at 105°C for 4 hours, cooled, and weighed. The insoluble lignin content was calculated using Equation (3), where ML is the lignin mass, and TL% is the lignin content.

$$TL\% = \left[\frac{ML}{MF}\right] \times 100 \quad (3)$$

d. Alpha-cellulose content
After the pineapple leaf fiber is treated with NaOH, it is filtered to remove soluble impurities with decantation. The fiber is then washed with 8.5% NaOH to purify it further and neutralize any remaining alkali. Next, acetic acid neutralizes excess NaOH, followed by a wash with distilled water to remove residual acid or contaminants. Finally, the fiber is dried in an oven at 105°C for 4 hours to remove moisture before weighing, allowing for calculating the fiber content. These washing and filtration steps ensure the fiber is correctly purified for accurate analysis. The sample was weighed, and the content was calculated using Equation (4), where MA is alpha-cellulose mass and TA% is alpha-cellulose content.

$$TA\% = \left[\frac{MA}{MF}\right] \times 100 \quad (4)$$

e. Particle Size Analyzer (PSA)
The cellulose nanocrystals that have been successfully synthesized were subjected to particle size distribution analysis using a Particle Size Analyzer instrument with model BIOBASE BK-802N and using detector HAMAMATSU photo-multiplier (5-90°C). The PSA is used to analyze the particle size of cellulose nanocrystals using the Dynamic Light Scattering (DLS) method. 0.25 mg of cellulose nanocrystals is weighed and placed into a cuvette, then aqua pro injection is added until it reaches 2.5 mg. The cuvette is then placed into the PSA holder.

f. X-Ray Diffraction (XRD)
XRD characterization was operated at 50 kV and 50 mA, equipped with Nickel-filtered Copper Kβ radiation (λ = 1,39 Å). The measurement was conducted by monitoring the diffraction angle 2θ at 5° to 50°. This method also allowed the analysis of the crystallinity index (CI) of the cellulose nanocrystals. CI was calculated using Equation (5).

$$\%CI = \frac{\text{Area of crystalline peaks}}{\text{Area of all peaks (crystalline+amorphouse)}} \times 100 \quad (5)$$

g. Fourier Transform Infrared Spectroscopy (FTIR)
The successfully fabricated cellulose nanocrystals were then subjected to functional group analysis using a Fourier Transform Infrared instrument. First, 3 mg of cellulose nanocrystals were weighed. Then, the sample was ground with 300 mg of potassium bromide (KBr). The sample and KBr mixture were pressed to form a pellet. The sample was then placed on a sample holder for measurement at a wavenumber range of 400–4000 cm^{-1}.

h. Scanning Electron Microscopy with Energy Dispersive X-Ray Spectroscopy (SEM-EDX)
The cellulose nanocrystals were then analyzed using SEM to determine their morphology before and after adsorption, while EDX was used to identify the elemental composition of the synthesized material. Before analysis, the sample was placed on

a carbon tape base and coated with Pd/Au for 15 minutes at a 6×10^{-2} mBar pressure.

4) Optimization of adsorption conditions

The adsorption conditions of cellulose nanocrystals for creatinine include specific parameters such as stirring speed, contact time, and feed solution concentration. These conditions are crucial for optimizing the efficiency of creatinine removal through adsorption, especially in the batch method.

a. Stirring speed optimization
Optimization of stirring speed was conducted with variations of 60, 100, 140, 180, and 210 rpm. 50 mg of CNC was added to 10 mL of a 10 mg/L creatinine solution. The mixture was then shaken for 30 minutes. The optimum stirring speed was determined from the highest values of q_{ads} and % removal from the measurements of the creatinine solution after adsorption. The formulas for calculating q_{ads} and % removal are given by Equation (6) and (7), where C_0 is initial concentration (mg/L), C_e is equilibrium concentration (mg/L), V is feed solution volume, and m is adsorbent mass.

$$q_{ads} = \frac{v}{m}(C_0 - C_e) \quad (6)$$

$$\%removal = \frac{C_0 - C_e}{C_0} \times 100\% \quad (7)$$

b. Contact time optimization
Optimization of contact time was performed with variations of 30, 60, 90, 120, 150, 180, and 210 minutes. 50 mg of CNC was added to 10 mL of a 10 mg/L creatinine solution. The mixture was then shaken at 210 rpm for the specified varying times.

c. Feed solution concentration optimization
Creatinine solution concentration was optimized with variations of 6, 8, 10, and 12 mg/L. At the specified concentrations, 50 mg of CNC was added to 10 mL of creatinine solution. The mixture was then shaken at 210 rpm for 120 minutes.

5) Determination of adsorption isotherm model

The adsorption isotherm model is determined by identifying the optimum concentration. The adsorption isotherm models used in this study are the Freundlich and Langmuir. The linearity of the determination coefficient (R^2) for each adsorption isotherm model can be determined through the following Equation (8) Freundlich and Equation (9) Langmuir, where K_F is the Freundlich constant or capacity factor ($mg^{1-1/n}L^{1/n}/g$), while 1/n is the Freundlich exponent. C_e is the equilibrium concentration (mg/L), q_e is the adsorption capacity (mg/g) at equilibrium, qm is the maximum adsorption capacity (mg/g), and K_L is the Langmuir isotherm constant (L/mg).

$$q_e = K_F C_e^{1/n} \quad (8)$$

$$q_e = \frac{q_m K_L C_e}{1 + K_L C_e} \quad (9)$$

6) Determination of adsorption kinetic model

The adsorption kinetic model is determined by identifying the optimum contact time between the adsorbent and adsorbate. In this study, the adsorption kinetics models used are pseudo-first-order and pseudo-second-order. The linearity of the determination coefficient (R^2) for each adsorption kinetics model can be determined through the following Equation (10) pseudo-first-order and Equation (11) pseudo-second-order, where q_e is adsorption capacity (mg/g) at equilibrium, q_t concentration of analyte adsorbed at time t, k_1 pseudo first order adsorption rate, and k_2 pseudo second order adsorption rate.

$$\log(q_e - q_t) = \log q_e - \frac{k_1}{2{,}303} t \quad (10)$$

$$\frac{t}{q_t} = \frac{1}{k_2 q_e^2} + \frac{1}{q_e} t \quad (11)$$

7) Biocompatibility test

This study conducted hemocompatibility testing through the Activated Partial Thromboplastin Time (APTT) test. A 4-channel semi-automated blood coagulation analyzer (Stago-STA Compact Max 3) was used for the APTT testing. A sample of 1 mg of the adsorbent was immersed in phosphate buffer saline (Diagnostica Stago) solution for 1 hour, incubated for 3 minutes at 37 °C together with 50 µL of platelet-poor plasma (PPP) and 50 µL of Actin FS (Diagnostica Stago). Subsequently, 50 µL of 0,025 M calcium chloride ($CaCl_2$) was added, and the blood coagulation time was observed.

Results and Discussion

Preparation and pretreatment

Before synthesizing CNC, pineapple leaf fiber needs to be prepared and pretreated to increase its cellulose content and reduce the levels of lignin, hemicellulose, and other non-cellulosic compounds (Randis *et al.*, 2024). The obtained pineapple leaf fiber is shown in Figure 1 (a), where the yellow-brown color indicates that many impurities are still present in the fiber.

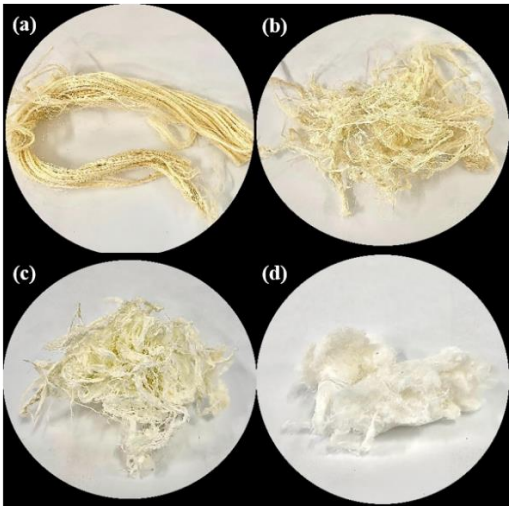

Figure 1. (a) Pineapple leaf fibers, (b) Mercerized fibers, (c) Bleached fibers, and (d) Delignified fibers

The pretreatment of pineapple leaf fiber consists of three stages: mercerization, bleaching, and delignification. Mercerization aims to remove lignin, hemicellulose, and other impurities within the fiber, which makes the cellulose fiber more visible *(*Siddiqui *et al.*, 2024). In this process, the color of the pineapple leaf fiber changes from yellow to pale yellow, as shown in Figure 1 (b). The second stage is bleaching, which removes the remaining lignin and hemicellulose from pineapple leaf fiber, making the cellulose fiber even more visible (Randis *et al.*, 2024). The bleached pineapple leaf fiber changes color from pale yellow to off-white, as shown in Figure 1 (c). The final stage is delignification, which aims to remove residual lignin in the pineapple leaf fiber after bleaching (Tsegaye *et al.*, 2019). The dignified pineapple leaf fiber changes color from off-white to white, as shown in Figure 1 (d). Besides the color changes, the effectiveness of the preparation and pretreatment process of pineapple leaf fiber was also demonstrated by the moisture, ash, lignin, and alpha-cellulose content found in Table 1.

Table 1. Test results for substance content in pineapple leaf fibers

Pineapple Leaf Fibers	Content			
	Moisture (%)	**Ash (%)**	**Lignin (%)**	**Alpha Cellulose (%)**
Before pretreatment	45.44	0.97	11.06	77.14
After pretreatment	4.28	0.44	5.57	91.28

Based on Table 1, the moisture content in the fiber decreased. This can be associated with a higher hemicellulose content in pineapple leaf fiber before pretreatment (Prado and Spinacé, 2019). The ash content in the fiber also decreased. The reduction in ash content after pretreatment is due to the removal of minerals during the bleaching process and repeated washing during extraction (Romruen *et al.*, 2022). The insoluble lignin content in the fiber also decreased, while the alpha-cellulose content increased. The reduction in lignin content and the increase in alpha-cellulose content result from the pretreatment process, which degrades the lignin present in pineapple leaf fiber, thereby yielding more free alpha-cellulose (Faria *et al.*, 2020).

Acid hydrolysis

The prepared and pretreated pineapple leaf fibers were then used for synthesizing CNCs through acid hydrolysis using H_2SO_4. The acid hydrolysis process can break down cellulose's disordered and amorphous regions, allowing individual cellulose crystals to become free. The hydronium ions in the acid break down the rigid structure of the cellulose fibers by attacking the glycosidic bonds, releasing individual crystallite (Santos *et al.*, 2013). The synthesized CNCs are white powder materials. The texture of cellulose nanocrystals is characterized by a light, slightly fibrous structure reminiscent of fine cotton. It has an exceptionally smooth surface, with a bright white color and a subtle, lustrous sheen, indicative of its high purity and crystalline organization. as shown in Figure 2. The results of this synthesis are shown in Figure 3, based on research from Bahadur *et al.* (2024). The nanocellulose exhibited a lighter fibrous structure with a glossy appearance. This transformation may be due to the breakdown of amorphous regions in the cellulose structure.

Figure 2. Synthesized cellulose nanocrystals

Figure 3. Synthesized cellulose nanocrystals from Mankamana-3 corncob biomass (Bahadur *et al.*, 2024)

Characterization

The particle size of the CNCs was analyzed using a Particle Size Analyzer, and the results can be seen in Figure 4. Figure 4 shows that the average particle size of the synthesized CNCs is 9.04 nm. Based on the tests using PSA, it is confirmed that the obtained material has a nanoscale size. This adsorbent falls within the nanoparticle category due to its 1–100 nm size range. The polydispersity index (PDI) obtained is 0.1070, indicating a high level of particle uniformity, as values between 0.1 and 0.7 generally suggest a well-homogenized nanosuspension. Studies have shown that a low PDI in this range enhances the stability of nanoparticle dispersions, potentially reducing agglomeration and improving adsorbent efficiency in applications like drug delivery and environmental remediation. Conversely, a PDI above 0.7 would indicate a broader particle size distribution, which increases the likelihood of sedimentation, a challenge frequently noted in nanoparticle formulations due to gravitational settling effects (Budiati *et al.*, 2021).

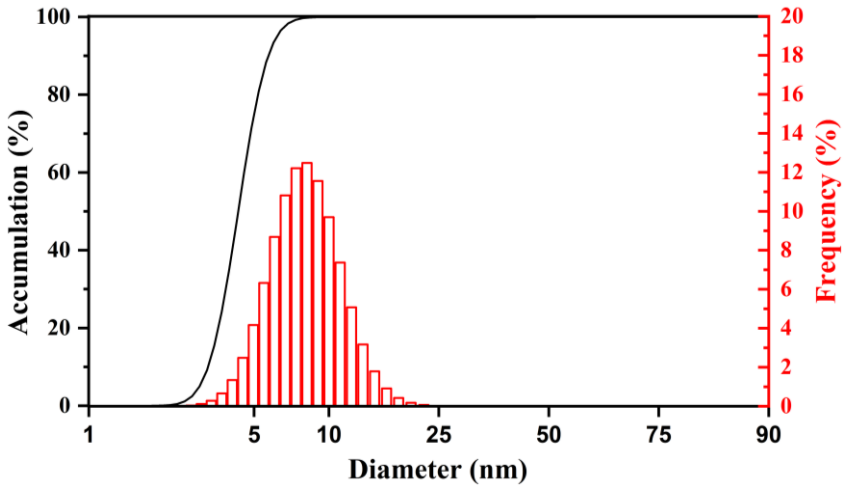

Figure 4. The particle size distribution results of cellulose nanocrystals

The XRD characterization results of the synthesized CNCs can be seen in Figure 5. Based on the peaks observed in the diffractogram, it is evident that CNCs have formed. This is supported by the correspondence of the diffractogram peaks between the synthesized CNCs and the JCPDS data number 00-056-1718. Figure 5 shows the diffractogram of the synthesized cellulose nanocrystals. In Figure 5, specific peaks can be seen at angles 2θ = 15.3°, 16.1°, 22.9°, and 34.7°.

These specific peaks also correspond to the characteristics of nanocellulose reported by Fujii *et al.* (2022). The crystallinity index of the synthesized cellulose nanocrystals is 76%. The crystallinity index of the synthesized cellulose nanocrystals is 76%. The crystallinity index of synthesized cellulose nanocrystals is similar to CNC from pepper waste (*piper nigrum L.*), has a crystallinity of 76.69% (Holilah *et al.*, 2024), CNC mesoporous hectorite bead has 76.8% (Holilah *et al.*, 2024), CNC from Mankamana-3 corncob has 66.55% (Bahadur *et al.*, 2024)

.

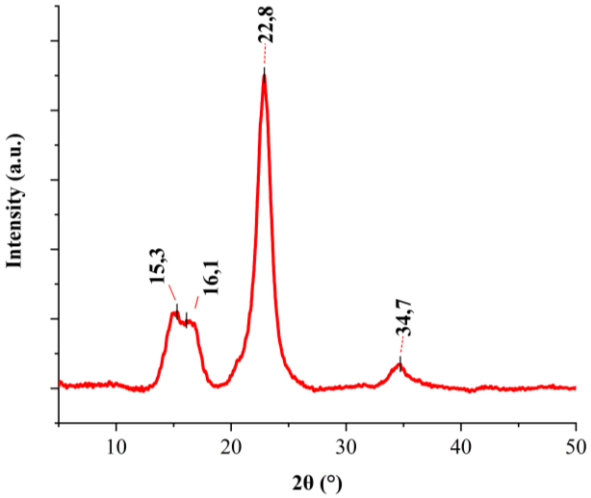

Figure 5. Diffractogram of cellulose nanocrystals

The functional group analysis of the synthesized CNCs was conducted using FTIR. The FTIR spectra of the CNCs are shown in Figure 6. Based on Figure 6, the successful synthesis of CNCs is indicated by absorption bands at wave numbers 3346.50 cm^{-1} and 2908.65 cm^{-1}, corresponding to hydroxyl (OH) and methylene (CH_2) groups, respectively. Additionally, absorption bands at 1371.39 cm^{-1} and 1058.92 cm^{-1} indicate the bending vibration of alcohol groups in CNCs and the symmetric stretching vibration of the C-O-C glycosidic bond or cellulose ring. These absorption peaks also align with those of nanocellulose reported by Prado and Spinacé (2019).

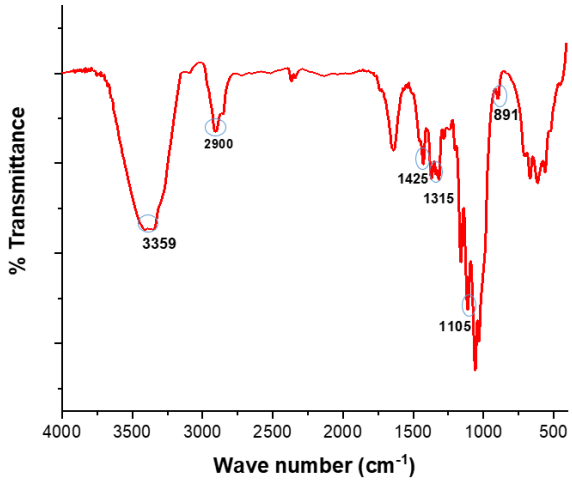

Figure 6. FTIR spectra of cellulose nanocrystals

The SEM images of the adsorbent before adsorption can be seen in Figures 7 (a) and (b), while the results after adsorption can be seen in Figures 7 (c) and (d). In Figure 7, differences in the surface morphology of the adsorbent before and after the adsorption process can be observed. The surface of the adsorbent appears smooth before adsorption, whereas after adsorption, it appears rougher. This change in surface morphology may result from interactions between the adsorbent surface and creatinine (Haghdoost *et al.*, 2021). In addition to SEM analysis, an EDX test was conducted to determine the atomic composition of the material. The EDX results are presented in Table 2, Table 3, Figure 8, and Figure 9.

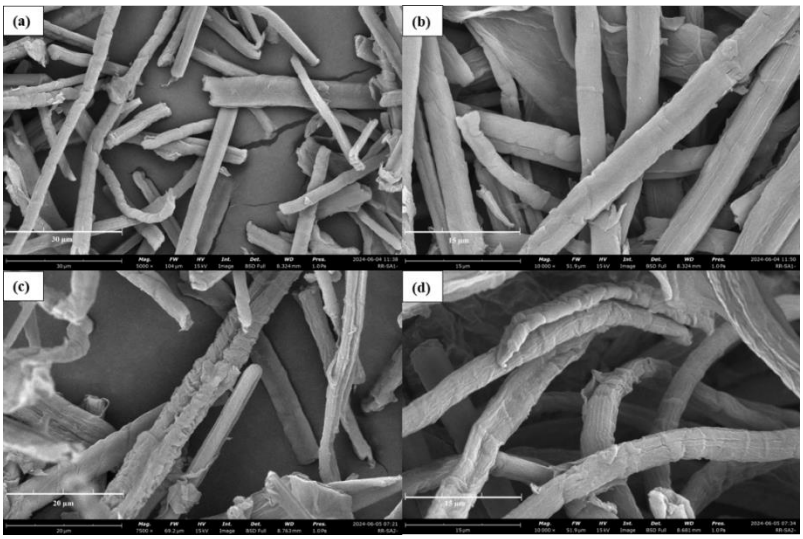

Figure 7. SEM image of cellulose nanocrystals before adsorption at magnifications (a) 5000×, (b) 10000×, and after adsorption at magnifications (c) 7500×, (d) 10000×

Table 2. Atomic composition of cellulose nanocrystals before adsorption

Element Number	Element Symbol	Element Name	Atomic Conc.	Weight Conc.
6	C	Carbon	67.699	60.899
8	O	Oxygen	32.060	38.600
14	Si	Silicon	0.241	0.501

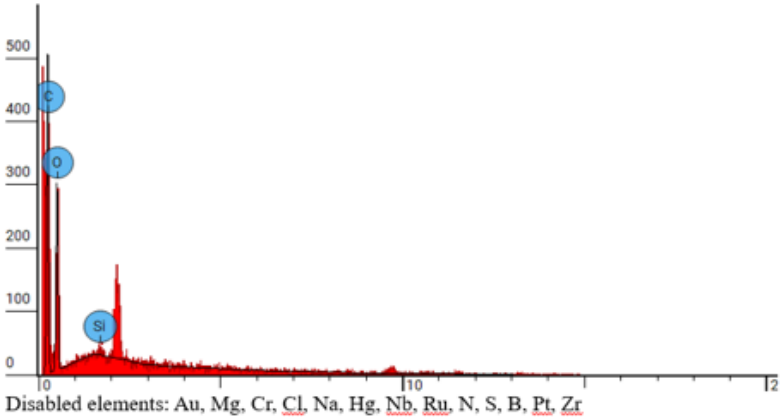

Figure 8. EDX results of cellulose nanocrystals before adsorption

Table 3. Atomic composition of cellulose nanocrystals after adsorption

Element Number	Element Symbol	Element Name	Atomic Conc.	Weight Conc.
6	C	Carbon	51.577	44.700
7	N	Nitrogen	5.737	5.800
8	O	Oxygen	42.439	49.000
14	Si	Silicon	0.247	0.500

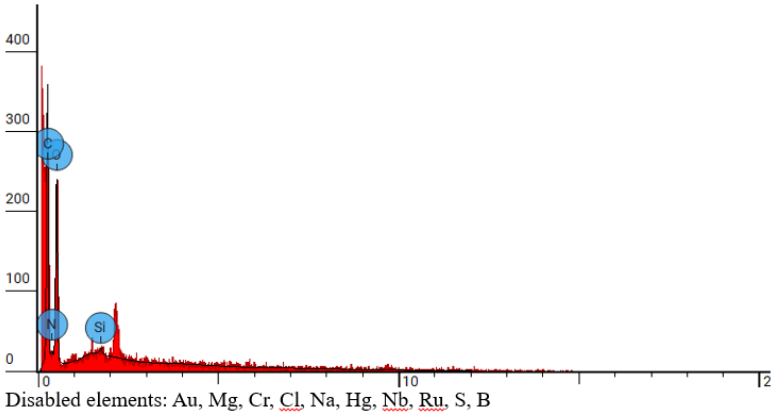

Figure 9. EDX results of cellulose nanocrystals after adsorption

Tables 2 and 3 show a clear difference in the CNCs before and after adsorption. The appearance of nitrogen (N) atoms in the CNC after adsorption indicates that creatinine has bound to the surface of the CNCs following the adsorption process. The nitrogen detected in the EDX results represents the nitrogen from the NH group in creatinine.

Optimization of adsorption conditions

Stirring speed is an important parameter to consider in batch adsorption systems. It helps distribute the adsorbent in all directions within the solution, allowing for thorough interaction with the adsorbate (Chouchane *et al.*, 2023). Figure 10 shows the relationship between stirring speed and both q_{ads} and %removal of creatinine by CNCs, indicating that the best adsorption occurs at a stirring speed of 210 rpm, with q_{ads} at 2.138 mg/g and %removal at 21.38%. The higher stirring speeds facilitate more effective contact between the adsorbate and adsorbent, enhancing adsorption capacity (Popaliya *et al.*, 2023).

Contact time is a crucial factor in the adsorption process, as it influences the interaction between the active sites on the adsorbent and the adsorbate (Nguyen *et al.*, 2021). Contact time can affect the interactions and attractive forces that form, such as Van der Waals and electrostatic forces (Nitsae *et al.*, 2021). As shown in Figure 11, both q_{ads} and %removal increase significantly with contact time and reaches equilibrium at a contact time of 120 minutes, with q_{ads} at 2.563 mg/g and %removal at 25.63%. This initial significant rise is due to the availability of free active sites on the adsorbent. In contrast, the slower increase is attributed to reduced available active sites as adsorption progress (Chouchane *et al.*, 2023).

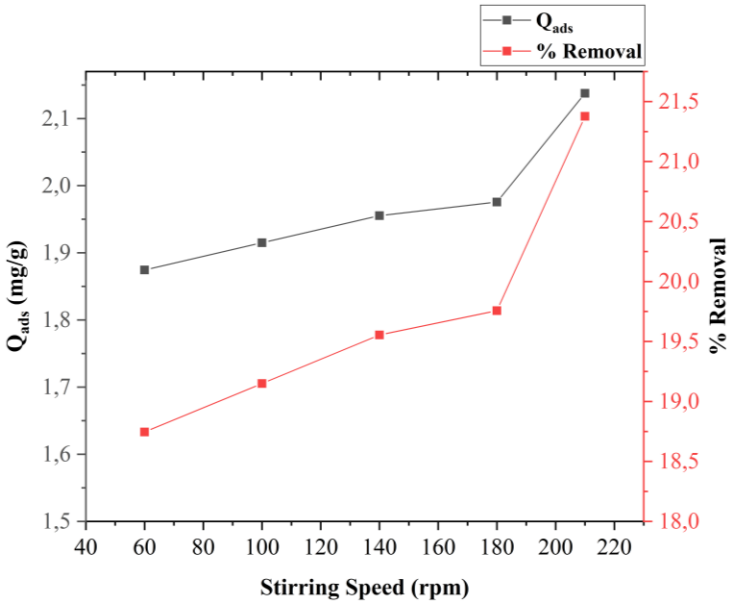

Figure 10. Effect of stirring speed in q_{ads} and %removal of creatinine

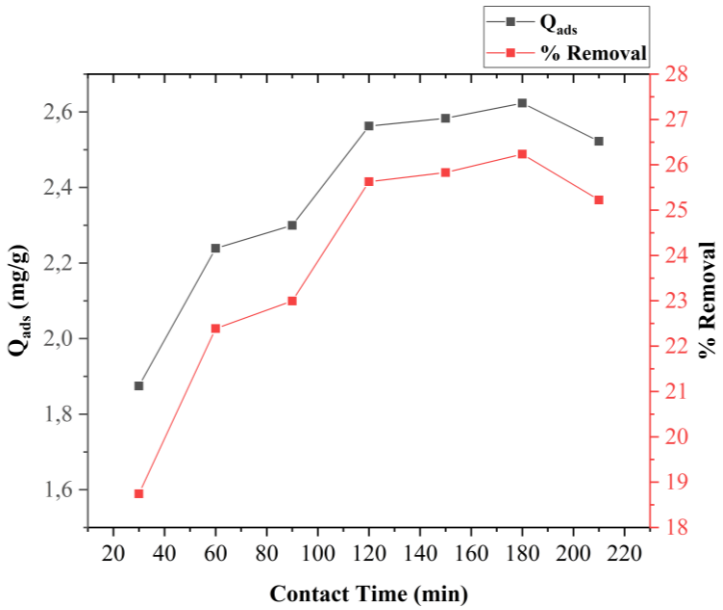

Figure 11. Effect of contact time in q_{ads} and %removal of creatinine

The feed solution concentration was determined to identify the maximum creatinine concentration that can be absorbed by 0.01 gram of cellulose nanocrystals adsorbent. As shown in Figure 12, the adsorption reaches optimal values at a concentration of 10 mg/L, with q_{ads} at 2.572 mg/g and %removal at 25.44%. This occurs because the active sites available on the adsorbent for creatinine adsorption are limited in number. Hence, these active sites become saturated at a particular adsorbate concentration and can no longer interact with additional adsorbate molecules (Popaliya *et al.*, 2023).

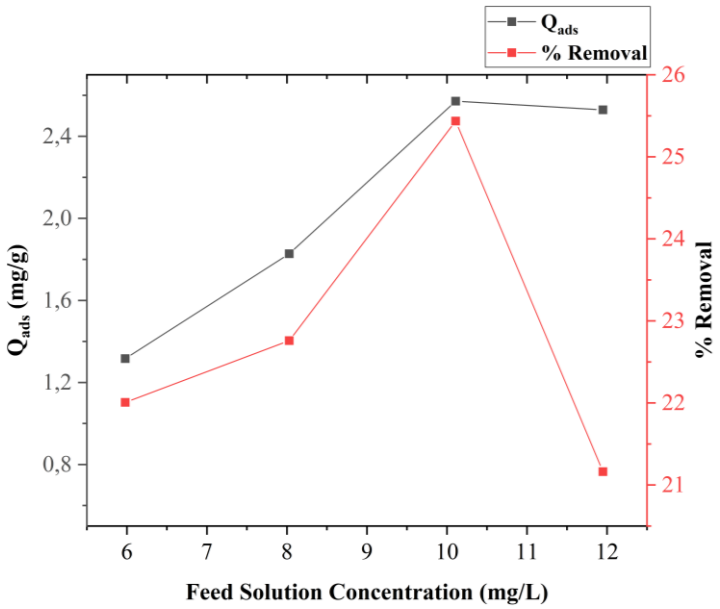

Figure 12. Effect of feed solution concentration in q_{ads} and %removal of creatinine

Determination of adsorption isotherm model

The determination of the kinetic model was based on the feed solution concentration influence data. Based on the data presented in Table 4, the R^2 value for the Freundlich isotherm model is closer to 1 than the Langmuir isotherm model. The Freundlich isotherm model indicates that the adsorbate layer formed on the adsorbent surface is multilayered (Raharjo *et al.*, 2019). In Table 4, the R_L values for nanocrystalline cellulose adsorbent fall within the range $0 < R_L < 1$, suggesting that creatinine adsorption using CNCs is favorable.

Table 4. Adsorption isotherm of cellulose nanocrystals

Sample	Langmuir				Freundlich		
	q_{max} (mg/g)	K_L (mL/g)	R_L	R^2	1/n	K_F (L/g)	R^2
Cellulose nanocrystals	9.5694	0.3834	0.2051	0.3484	0.7981	0.4408	0.9158

Determination of adsorption kinetic model

The kinetic model was determined based on the data of contact time influence. According to Table 5, creatinine adsorption using CNCs adsorbent best fits the pseudo-second-order kinetic model, as indicated by the R^2 value being closer to 1 than the pseudo-first-order model. Adsorption following a pseudo-second-order kinetic model indicates that adsorption of the adsorbate on the active sites of the adsorbent occurs through a chemical process, forming a stable chemical bond between the adsorbate and adsorbent (Muliwa *et al.*, 2023). Adsorbents used for hemoperfusion applications must have a high affinity for uremic toxins in the blood. Table 6 presents some data showing the creatinine adsorption capacity of adsorbents from previous studies and this study.

Table 5. Adsorption kinetic of cellulose nanocrystals

Sample	Pseudo first order			Pseudo second order		
	q_e (mg/g)	K_1 (1/min)	R^2	q_e (mg/g)	K_2 (1/min)	R^2
Cellulose nanocrystals	0.7792	0.0138	0.6084	2.7601	0.0267	0.9958

Table 6. Comparison of the creatinine adsorption capacity of adsorbents from previous studies and this study

Adsorbent type	Maximum adsorption capacity	Reference
MIL-100(Fe)	30 mg/g	(Yang *et al.*, 2014)
Poly (ethylene-co-vinyl alcohol) (EVOH)-zeolite–polymer composite nanofibers	25 mg/g	(Namekawa *et al.*, 2014)
Dialdehyde nanofibrillated cellulose	6.7 mg/g	(Cui *et al.*, 2016)
Heparin-mimicking polymers grafted carbon nanotube/poly (ethersulfone) composite	1.4 mg/g	(Nie *et al.*, 2015)
Creatinine-imprinted poly (tetraethoxysilanol) sol–gel	0.8 mg/g	(Tsai and Syu, 2011)
Cellulose nanocrystals	2.57 mg/g	This study

Biocompatibility test

The blood coagulation time test was conducted to evaluate the hemocompatibility of the adsorbent when in direct contact with blood. The APTT test results are shown in Figure 13. In the control, the blood clotting results were obtained for 30.4 seconds, whereas when contacted with the sample, it was extended to 31.3 seconds. These results indicate that the CNCs adsorbent sample has a coagulation time close to the control blood sample. This favorable outcome proves that the adsorbent material is safe and does not cause excessive blood clotting. Normal APTT values range between 25–36 seconds, or 1.5–2.0 times the APTT time of the control sample (Yildirim *et al.,* 2013). The synthesized CNCs adsorbent is still within the normal APTT range. Supporting literature, such as guidelines from ISO 10993-4 on blood compatibility, emphasizes the importance of testing biomaterials for safe integration, as blood-contacting materials should not disrupt red or white blood cells, nor should they activate coagulation pathways in a way that could lead to unintended clotting or immune responses. Additionally, research shows that hemocompatibility assessments using both static and dynamic models can provide a robust evaluation, as these simulate actual blood flow conditions and help predict in vivo outcomes for biomaterial applications, ensuring a safer profile in medical contexts (Strohbach and Busch, 2021; Weber *et al.,* 2018).

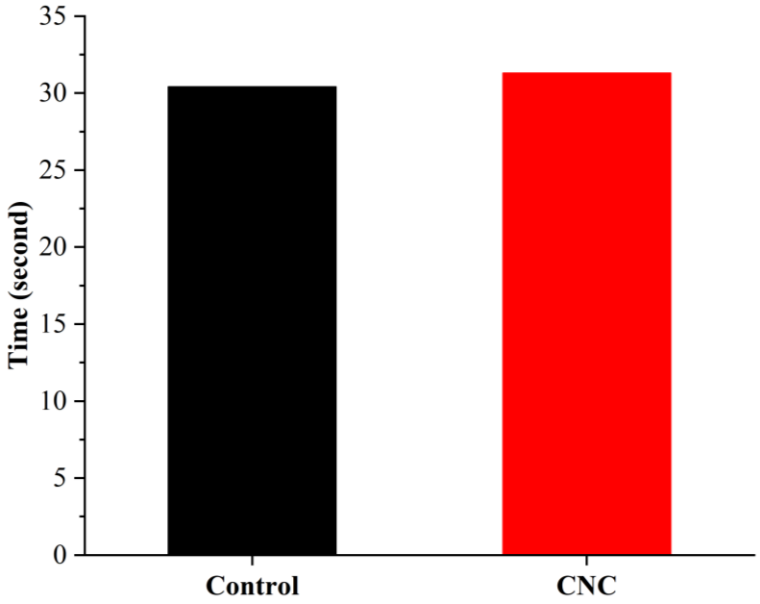

Figure 13. APTT test results

Conclusions

The CNCs synthesized from pineapple leaf fibers have a particle size of 9.04 nm and crystallinity index of 76%. The optimal conditions for creatinine adsorption using CNCs were achieved with stirring speed of 210 rpm, contact time of 120 minutes, and feed solution concentration of 10 mg/L with %removal of creatinine 25,44%. The APTT test results for the CNCs indicate that the sample made from pineapple leaf fiber had coagulation time comparable to the control blood sample, which was extended for 1.3 seconds. This confirms that CNCS are safe and does not induce excessive blood clotting. CNCs synthesized from pineapple leaf fibers can be developed for hemoperfusion applications as an environmentally friendly adsorbent. However, CNC's adsorption capacity is relatively small, so the adsorbent needs additional modification, both physically and chemically.

Acknowledgment

The authors would like appreciate to Universitas Airlangga for funding by SATU Joint Research Scheme (No: 1254/UN3.15/PT/2022).

Conflict of Interest

The authors declare that have no conflict of interest.

References

Alfonso, A.A., Mongan, A.E. and Memah, M.F., 2016. Gambaran kadar ureum pada pasien penyakit ginjal kronik stadium 5 non dialisis. *Jurnal e-Biomedik*, 4(2), pp.2–7.

Budiati, A., Rahmat, D. and Alwiyah, Z., 2021. Aktivitas Antioksidan dan Tabir Surya Nanopartikel Ekstrak Rimpang Temulawak (Curcuma Xanthorrhiza Roxb .) dan Formulasi dalam Bentuk Krim. *Jurnal Jamu Indonesia*, 6(2), pp.75–83.

Chouchane, T., Boukari, A., Khireddine, O., Chibani, S. and Chouchane, S., 2023. Equilibrium, kinetics, and thermodynamics of batch adsorption of Mn(II) ions on blast furnace slag (BFS) and kaolin (KGA). *Journal of Engineering and Applied Science*, 70(1).

Cui, D., Liu, Z., Yang, Y., Huang, R., Cheng, X., Fatehi, P. and Sun, B., 2016. Adsorption performance of creatinine on dialdehyde nanofibrillated cellulose derived from potato residues. *Biotechnology Progress*, 32(1), pp.208–214.

Faria, L.U.S., Pacheco, B.J.S., Oliveira, G.C. and Silva, J.L., 2020. Production of cellulose nanocrystals from pineapple crown fibers through alkaline pretreatment and acid hydrolysis under different conditions. *Journal of Materials Research and Technology*, 9(6), pp.12346–12353.

Fujii, E., Furutani, M., Kimura, Y. and Ogura, K., 2022. Single-Step Synthesis of Silver Nanoparticles Supported on Cellulose Nanofibers Using a High-Pressure Wet-Type Jet Mill and Their Catalytic Activities. *Materials Transactions*, 63(5), pp.748–751.

Gadzama, S.W., Sunmonu, O.K., Isiaku, U.S. and Danladi, A., 2020. Isolation and characterization of nanocellulose from pineapple leaf fibres via chemo-mechanical method. *Science World Journal*, 15(2), pp.100–105.

Haghdoost, F., Bahrami, S.H., Barzin, J. and Ghaee, A., 2021. Preparation and characterization of electrospun polyethersulfone/polyvinylpyrrolido ne-zeolite core–shell composite nanofibers for creatinine adsorption. *Separation and Purification Technology*, 257.

Holilah, H., Suryanegara, L., Bahruji, H., Hamid, Z.A.A., Wahyudi, M.S., Masruchin, N., Asranudin, A., Faradilla, R.F., Syafri, E., Melenia, A.T., Jovita, S., Nugraha, R.E. and Prasetyoko, D., 2024. Reusability of lactic acid on hydrolysis of nanocrystalline cellulose from pepper waste (piper nigrum L.). *Case Studies in Chemical and Environmental Engineering*, 10(August), p.100922.

Jiang, H., Wu, S. and Zhou, J., 2023. Preparation and modification of nanocellulose and its application to heavy metal adsorption: A review. *International Journal of Biological Macromolecules*, 236(February), p.123916.

Kovesdy, C.P., 2022. Epidemiology of chronic kidney disease: an update 2022. *Kidney International Supplements*, 12(1), pp.7–11.

Levey, A.S. and Coresh, J., 2012. Chronic kidney disease. *The Lancet*, 379(9811), pp.165–180.

Li, C., Zhang, X., Bao, C., Zhang, J., Tian, Y., Shen, J. and Feng, X., 2022. Freezing-induced chemical crosslinking to fabricate nanocellulose-based cryogels for efficient bilirubin removal. *Separation and Purification Technology*, 300(May), p.121865.

Lim, K.Y. and Foo, K.Y., 2024. Facile preparation of multifunctional cellulose nanocrystals from coffee residue via hydrothermal technique: Prolific roles on the water purification, antibacterial and antifungal applications. *Journal of Water Process Engineering*, 67(October).

Muliwa, A.M., Oyewo, O.A. and Maity, A., 2023. Recent progress on the removal of aqueous mercury by carbon-based adsorbents: A review. *Inorganic Chemistry Communications*, 156.

Namekawa, K., Tokoro Schreiber, M., Aoyagi, T. and Ebara, M., 2014. Fabrication of zeolite-polymer composite nanofibers for removal of uremic toxins from kidney failure patients. *Biomaterials Science*, 2(5), pp.674–679.

Nguyen, C.H., Fu, C.C., Chen, Z.H., Tran, T.T. Van, Liu, S.H. and Juang, R.S., 2021. Enhanced and selective adsorption of urea and creatinine on amine-functionalized mesoporous silica SBA-15 via hydrogen bonding. *Microporous and Mesoporous Materials*, 311.

Nie, C., Ma, L., Xia, Y., He, C., Deng, J., Wang, L., Cheng, C., Sun, S. and Zhao, C., 2015. Novel heparin-mimicking polymer brush grafted carbon nanotube/PES composite membranes for safe and efficient blood purification. *Journal of*

Membrane Science, 475, pp.455–468.

Nitsae, M., Solle, H.R.L., Martinus, S.M. and Emola, I.J., 2021. Studi adsorpsi metilen biru menggunakan arang aktif tempurung lontar (Borassus flabellifer L.) asal Nusa Tenggara Timur. *Jurnal Kimia Riset*, 6(1), pp.46–57.

Popaliya, M.R., Mishra, M. and Mishra, A., 2023. Removal of cationic dyes onto java plum leaves ash: adsorption isotherms, kinetics, thermodynamic and characterizations. *Chemical Papers*, 77(12), pp.7881–7901.

Prado, K.S. and Spinacé, M.A.S., 2019. Isolation and characterization of cellulose nanocrystals from pineapple crown waste and their potential uses. *International Journal of Biological Macromolecules*, 122, pp.410–416.

Raharjo, Y., Ismail, A.F., Othman, M.H.D., Malek, N.A.N.N. and Santoso, D., 2019. Preparation and characterization of imprinted zeolite-Y for p-cresol removal in haemodialysis. *Materials Science and Engineering C*, 103.

Rajendra Bahadur, G.C., Awasthi, G.P., Shin, M., Sharma, K.P., Neupane, B.B., Kalauni, S.K., Bhattarai, N., Yu, C. and Joshi, M.K., 2024. Nanocellulose from Mankamana-3 corncob biomass: Synthesis, characterization, surface modification and potential applications. *Bioresource Technology Reports*, 28(October), p.101971.

Randis, R., Darmadi, D.B., Gapsari, F. and Sonief, A.A.A., 2024. Isolation and characterization of microcrystalline cellulose from oil palm fronds biomass using consecutive chemical treatments. *Case Studies in Chemical and Environmental Engineering*, 9.

Romruen, O., Karbowiak, T., Tongdeesoontorn, W., Shiekh, K.A. and Rawdkuen, S., 2022. Extraction and Characterization of Cellulose from Agricultural By-Products of Chiang Rai Province, Thailand. *Polymers*, 14(9).

Santos, R.M. dos, Flauzino Neto, W.P., Silvério, H.A., Martins, D.F., Dantas, N.O. and Pasquini, D., 2013. Cellulose nanocrystals from pineapple leaf, a new approach for the reuse of this agro-waste. *Industrial Crops and Products*, 50, pp.707–714.

Saragih, H.T.M., Sembiring, J.H. and Ginting, E., 2023. Conversion of Pineapple Peel Glucose Into Bioethanol Using Simultaneous Saccharification and Fermentation (Ssf) Method and Separate Hydrolysis and Fermentation (Shf) Method. *Jurnal Kimia Riset*, 8(2), pp.167–174.

Siddiqui, V.U., Almehjani, T.M., Sapuan, S.M., Jamal, T., Ilyas, R.A., Eldin, S.M., Khan, A. and Jameel, Y., 2024. Isolation and Characterization of Cellulose from Pomegranate (Punica granatum) Peel. *Journal of Natural Fibers*, 21(1).

Strohbach, A. and Busch, R., 2021. Predicting the in vivo performance of cardiovascular biomaterials: Current approaches in vitro evaluation of blood-biomaterial interactions. *International Journal of Molecular Sciences*, 22(21).

Sun, B., Hou, Q., He, Z., Liu, Z. and Ni, Y., 2014. Cellulose nanocrystals (CNC) as carriers for a spirooxazine dye and its effect on photochromic efficiency. *Carbohydrate Polymers*, 111, pp.419–424.

Tsai, H.A. and Syu, M.J., 2011. Preparation of imprinted poly(tetraethoxysilanol) sol-gel for the specific uptake of creatinine. *Chemical Engineering Journal*, 168(3), pp.1369–1376.

Tsegaye, B., Balomajumder, C. and Roy, P., 2019. Alkali delignification and

Bacillus sp. BMP01 hydrolysis of rice straw for enhancing biofuel yields. *Bulletin of the National Research Centre*, 43(1).

Wang, T., Gu, W., Yu, L., Guo, X., Yang, J., Sun, X., Guan, J., Zhou, L., Wang, C., Yao, H., Zhang, X. and Wang, G., 2023. MXene: An efficient hemoperfusion sorbent for the removal of uremic toxins. *Journal of Materiomics*, 9(6), pp.1129–1140.

Weber, M., Steinle, H., Golombek, S., Hann, L., Schlensak, C., Wendel, H.P. and Avci-Adali, M., 2018. Blood-Contacting Biomaterials: In Vitro Evaluation of the Hemocompatibility. *Frontiers in Bioengineering and Biotechnology*, 6(July).

Yang, C.X., Liu, C., Cao, Y.M. and Yan, X.P., 2014. Metal-organic framework MIL-100(Fe) for artificial kidney application. *RSC Advances*, 4(77), pp.40824–40827.

Yildirim, A., Ozgur, E. and Bayindir, M., 2013. Impact of mesoporous silica nanoparticle surface functionality on hemolytic activity, thrombogenicity and non-specific protein adsorption. *Journal of Materials Chemistry B*, 1(14), pp.1909–1920.